World Scientific
www.worldscientific.com

Terahertz wave detection by plasmonic-antenna enhanced sum frequency generation

Jie Sun[*], Fangxing Zhang[†], Zhihao Zhou[†], Dongyi Shen[*],
Qiao Kang[*], Xin Luo[†], Guolin Zhao[*],
Wei Liu[*] and Wenjie Wan[*,†,‡]

[*]*The State Key Laboratory of Advanced*
Optical Communication Systems and Networks,
School of Physics and Astronomy,
Shanghai Jiao Tong University,
Shanghai 200240, P. R. China

[†]*MOE Key Laboratory for Laser Plasmas and Collaborative*
Innovation Center of IFSA
University of Michigan-Shanghai
Jiao Tong University Joint Institute
Shanghai Jiao Tong University,
Shanghai 200240, P. R. China
[‡]*wenjie.wan@sjtu.edu.cn*

We propose a scheme of terahertz (THz) indirect detection via plasmonic-antenna enhanced sum frequency generation process, where the THz wave is converted to optical wave that is detected by photodetector. The gold antenna built in the structure can improve the conversion efficiency by enhancing both the optical wave and THz wave. The numerical simulations show that the field enhancement is influenced by the geometry of the antenna, so the conversion efficiency can be improved highly by optimizing the antenna. Compared with commercial detectors, our detection system has a much lower noise equivalent power (NEP) of $15.4\,\mathrm{pW}/\sqrt{\mathrm{Hz}}$ at 5 THz.

Keywords: Nonlinear optics; sum frequency generation; terahertz waves; plasmonics.

1. Introduction

Terahertz wave is located in the gap of microwave and infrared light, and it is usually researched in the cross-discipline consisting of electronics and photonics. In recent years, terahertz technology captures more and more attention by researchers because of its extensive and potential applications in many important fields, such as communication,[1] internet of things,[2] biological and medical research,[3] food quality

‡Corresponding author.

inspection,[4] security and environmental monitoring.[5] In particular, the rapid surge in wireless communications creates a demanding requirement for the next generation communication platform such as 6G in term of its speed, spectrum and bandwidth,[6,7] where the carrier frequency determines the upper limit of the bandwidth, well-known as the Shannon limit in information theory.[8] Fortunately, terahertz wave can provide bandwidth up to several THz and expand the capacity of wireless systems, and thus the higher speed wireless communication is envisioned to be realized.[9,10] Although terahertz technology has a wide range of applications, there remain many challenges to be solved, such as radiation sources, detectors and transmission lines.[11]

As one of the core technologies of terahertz science, THz detectors are crucial in THz application systems and have been extensively investigated.[12–14] In current main THz detectors, thermal detectors such as semiconductor bolometers, pyroelectric detectors and Golay cells are low-cost and widely used for broadband detection, but lack high responsivity, and most semiconductor bolometers (e.g., InSb bolometers) usually require low-temperature operation.[12,15,16] THz time-domain spectroscopy (THz-TDS) detection systems such as photoconductive antennas are commonly used in pulsed THz detection, which can operate in room-temperature environment and possess high stability, but are complicated and expensive when operating in broad-bandwidth.[12,17] Heterodyne detectors such as Schottky Barrier Diode (SBD), Superconductor-Insulator-Superconductor (SIS), Hot Electron Bolometer (HEB) have high responsivity and low NEP, but require operations below liquid helium temperature, and these mixer structures inevitably complicate the equipment and increase the cost.[13,14] Single photon detectors and terahertz quantum-well photodetectors have advantages of outstanding sensitivity and extremely low NEP, but need to be cooled to liquid helium temperature, which makes them expensive and difficult to use.[13,18–20] These problems such as low-temperature operating environment, low sensitivity and complexity have impacted the flexible applications of THz detectors in more extensive fields.

Owing to these difficulties in current THz detectors, a novel detection scheme based on frequency up-conversion has been proposed in the past.[21–24] In this scheme, THz signal can be converted into optical domain through sum frequency generation (SFG) process in the nonlinear material with a dielectric $\chi^{(2)}$ such as $LiNbO_3$ crystal, and the THz signal can be detected indirectly through receiving the generated optical signal with high sensitive Near-Infrared (NIR) photodetectors such as avalanche photodiode (APD). The scheme of THz detection is a promising approach for its simplicity, wide tunability and capability of frequency conversion from THz to infrared. Therefore, it can make up for the shortages of current commercial THz detectors. Further, this scheme combines THz domain and optical domain, so it can also provide a significant proposal to integrate the THz wireless link into fiber-optic network for future wireless communication establishment.[9,25]

However, due to the limitation of THz sources in actual applications, the intensity of THz signal to be detected is usually feeble. On the other hand, the conversion efficiency of the nonlinear process is also very low.[26,27] These problems make the

intensity of the generated optical signal much little and hard to detect. A general route is to improve the intensity of incident waves interacting in the nonlinear process, leading to the enhanced output intensity of the generated wave. In previous work, we proposed an efficient terahertz generation scheme based on nonlinear difference frequency generation (DFG) with a metallic nanostructure, in which the surface plasmons are excited to enhance the interacting light waves.[28] Inspired by this work, we can design metallic structures such as plasmonic antennas to enhance the electric field. However, most of the nanoantennas previously studied are used to enhance optical wave, but have little effect on THz wave, which limits the possibility of higher conversion efficiency.[29,30] Therefore, it is promising and significant to enhance both optical wave and THz wave at the same time with proper structures for obtaining higher conversion efficiency and higher intensity of the generated wave.

In this paper, we propose a new detection scheme based on the SFG process with a structure consisting of gold antenna and second-order nonlinear $LiNbO_3$ crystal, which ensures that the detector can operate with high conversion efficiency and wide bandwidth at room temperature. The dependence of the enhancement of incident waves in optical domain and THz domain on the geometrical parameters of gold antenna has been studied with numerical simulations by using the finite element analysis (FEA) method. We show that both the optical wave and THz wave can be enhanced by the gold antenna mainly based on the localized surface plasmon resonance (LSPR) and antenna effect, respectively. Further, we simulate the SFG process of optical wave and THz wave by utilizing the finite-difference time-domain (FDTD) method. We also discuss the conversion efficiency of this scheme, and the simulation results show that the unique structure enables the detection system to achieve low NEP benefiting from high-sensitive photodetector.

2. THz Detection Scheme Based on SFG Process

We start with the description of mechanisms of enhancement on the optical wave and THz wave interacting in the nonlinear SFG process. Traditionally, the optical wave incident on noble metals such as gold and silver nanoparticles can lead to the excitation of LSPR for high plasma frequencies and electrical conductivity of metals, and the electric field is confined and enhanced highly surrounding the hotspots of metallic nanostructures.[31–33] In addition, the optical properties of the metallic nanostructures depend on their dimensions and shapes.[34,35] However, in THz regime, the metal serves as perfect electric conductor that is different from in optical regime, so the interaction between THz wave and metallic nanostructures cannot support the LSPR mode and field enhancement.[36] Nevertheless, based on the antenna effect, the gold antenna can be tailored and designed with proper parameters (e.g., the length of the antenna should be on the order of THz wavelength to couple the incident energy) to enhance the incident THz wave. Further, the sharp tips of the antenna can also lead to the enhancement of incident waves based on the lightning rod effect, which will be discussed in the following sections.
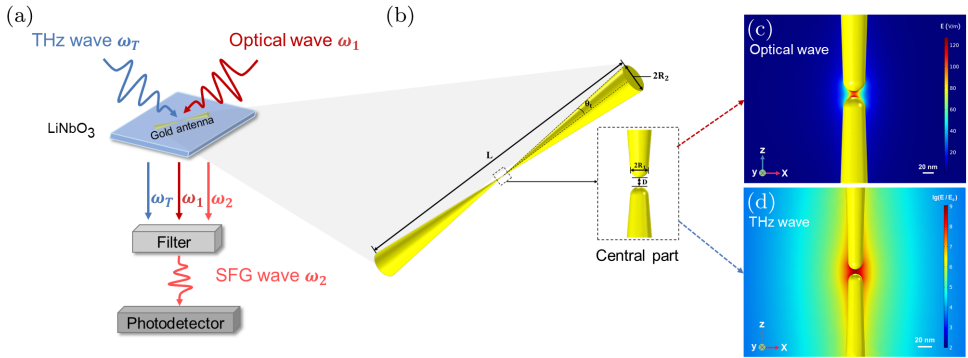
Fig. 1. Schematic illustration of the THz detector. (a) The THz detection system and fundamental process. The THz wave ω_T and optical wave ω_1 are enhanced by the gold antenna based on different enhancement effects, respectively. The optical wave with a new frequency of ω_2 is generated by SFG process. The optical filter only permits the optical wave at ω_2 to propagate and be received by the photodetector. (b) Sketch of the antenna and definition of geometrical parameters. The antenna consists of cones and hemispheres. L is the total length of the antenna; θ_t is the half angle of the cone; R_2 is the bottom radius of the cone. The inset in the dashed frame zooms in the central part of the antenna, where D is the gap distance between cones; R_1 is the tip radius of the antenna. (c) The enhanced optical field distribution E surrounding the tips of antenna simulated with FEA method, and the optical wave propagates along the x-axis with polarization parallel to the z-axis. (d) The enhanced THz field exponential distribution lg (E/E_0) $(E_0 = 1 \text{ V/m})$ surrounding the central part of the antenna simulated with the FEA method, and the THz wave propagates along the x-axis with polarization parallel to the z-axis.

A schematic of the technological step used for THz detection is shown in Fig. 1(a). In our scheme, the LiNbO$_3$ crystal provides the nonlinearity for the SFG process, in which the gold antenna is designed with proper geometrical parameters including length, gap distance, radius, etc. The optical wave at ω_1 and THz wave at ω_T are inputted into the LiNbO$_3$ crystal and close to the gap of the antenna to achieve greater amplification. The new optical wave at the frequency of ω_2 $(\omega_2 = \omega_1 + \omega_T)$ is generated in SFG process, and the optical filer is used to transmit light ω_2 and block light ω_1. Finally, the light ω_2 is received by the high-sensitive photodetector to detect THz wave indirectly.

Fig. 1(b) presents the sketch of the antenna and definition of geometrical parameters. As shown in Fig. 1(b), the tip of the cone is set to hemisphere instead of vertex, which is corresponding to the actual geometry and avoids singularities in the simulation. Controllable geometrical parameters include the total length L of the antenna, the half angle θ_t of the cone; the bottom radius R_2 of the cone, the gap distance D between the cone, and the tip radius R_1 of the antenna. In the following sections, we will explore the dependence of the electric field enhancement on the geometry of the antenna.

In order to reveal the different enhancement effects in optical regime and THz regime, Figs. 1(c) and 1(d) demonstrate the enhanced electric field distribution of optical wave and THz wave around the center of the antenna, respectively, which are simulated with the FEA method. As shown in Fig. 1(c), the antenna collects the

energy of the incident optical wave and converts it into concentrated energy due to the excitation of LSPR; therefore, the electric field is localized and highly enhanced at the gap. However, different from Fig. 1(c), Fig. 1(d) shows that the THz field surrounding the center of the antenna is not confined at the gap but radiates with enhanced energy, which demonstrates the antenna resonance due to the induced electric dipole oscillations in antenna. More detailed discussions about the enhancement effect in optical domain and THz domain will be given in the following sections with numerical simulation.

3. Results and Discussion

3.1. *Numerical simulation of optical field enhancement*

We firstly consider the enhancement process of the optical field simulated by the FEA method. In the telecommunications industry, the reliable systems operating at 1550 nm are commercially available and cost-effective. Therefore, in order to achieve compatibility with the applications in current telecommunication systems, we use the laser source emitting at 1,550 nm for numerical simulation.[37] Meanwhile, we choose Au as the material of the antenna for plasmonic, which performs well at low NIR frequency and is relatively stable in natural environment,[34] and the dielectric constants of Au in optical regime are taken from Ref. 38. In addition, because the length of the whole antenna is on the order of THz wavelength and much longer than 1,550 nm, in order to reduce the computational memory and avoid non-convergence in simulation software, we take the central part of the antenna for simulation in optical domain without affecting the optical properties of the antenna, and the length can be close to the order of light wavelength.[39]

The calculated electric field distribution surrounding the tip of the antenna is illustrated in Fig. 2(a). The geometrical parameters of the simulated antenna are $L = 1.15 \,\mu\text{m}$, $D = 10 \,\text{nm}$, $R_1 = 10 \,\text{nm}$ and $\theta_t = 1.89°$. The incident optical wave at 1,550 nm propagates along the x-axis perpendicular to the antenna with the polarization parallel to the antenna. For simplicity, the initial amplitude E_0 of the incident wave is set to 1 V/m, and E denotes the maximum of the enhanced electric field, so E/E_0 represents the field enhancement. As shown in Fig. 2(a), the electric field is confined at the gap of the antenna and can be enhanced greatly up to two orders of magnitude due to the excitation of LSPR.[30]

The LSPR properties of metallic nanostructures is highly dependent on their shapes, so the field enhancement can be optimized through tunning the geometry of the structure.[39,40] Figs. 2(b)–2(d) show that the field enhancement E/E_0 is influenced by the geometry of the antenna, including the gap distance D, the tip radius R_1 and the half angle θ_t. In these simulations, the initial parameters are $L = 1.15 \,\mu\text{m}$, $D = 10 \,\text{nm}$, $R_1 = 10 \,\text{nm}$ and $\theta_t = 1.89°$, and then changed respectively (marked with red color in insets). As shown in Fig. 2(b), the field enhancement E/E_0 decreases with increasing gap distance D, and the electric field can be enhanced up to three
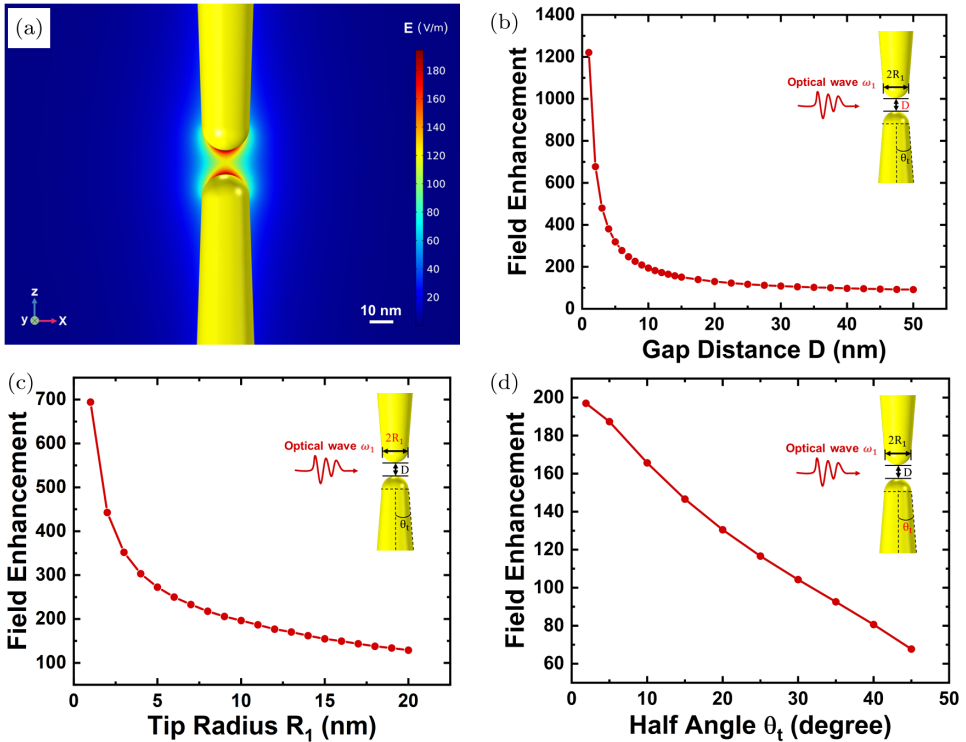
Fig. 2. (Color online) Numerical simulation of optical field enhancement. (a) The cross-section of the electric field distribution surrounding the tip of the antenna in the plane containing the propagation and polarization axes. Especially, the electric field is confined and enhanced in the gap. (b)–(d) show the field enhancement E/E_0 versus geometrical parameters of antenna, including (b) the gap distance D, (c) the tip radius R_1 and (d) the half angle θ_t. Insets in (b)–(d) show the schematics of the simulated model with changed parameter (marked with red color) and unchanged parameters (marked with black color). In these simulations, the initial parameters are $L = 1.15\,\mu$m, $D = 10$ nm, $R_1 = 10$ nm and $\theta_t = 1.89°$.

orders of magnitude when the gap distance is 1 nm. Fig. 2(c) shows that as the tip radius R_1 decreases, the field enhancement increases, which demonstrates that the field enhancement is also influenced by the lightning rod effect due to the sharp-pointed tip.[41,42] In addition, the antenna can be considered as bow-tie antenna, of which the field enhancement is affected by the half angle θ_t. The results shown in Fig. 2 (d) reveal that the enhancement decreases as the half angle θ_t increases, and achieves the maximum when the half angle approaches to zero, which is consistent with other researches on optical field enhancement based on bow-tie antenna.[39,43]

3.2. *Numerical simulation of THz field enhancement*

In this section, we simulate the enhancement process of the terahertz field with the FEA method. In this simulation, we adopt the wavelength-dependent dielectric constants of Au in THz regime from Ref. 44. The calculated electric field distribution around the antenna is illustrated in Fig. 3(a). Same as optical wave, the incident
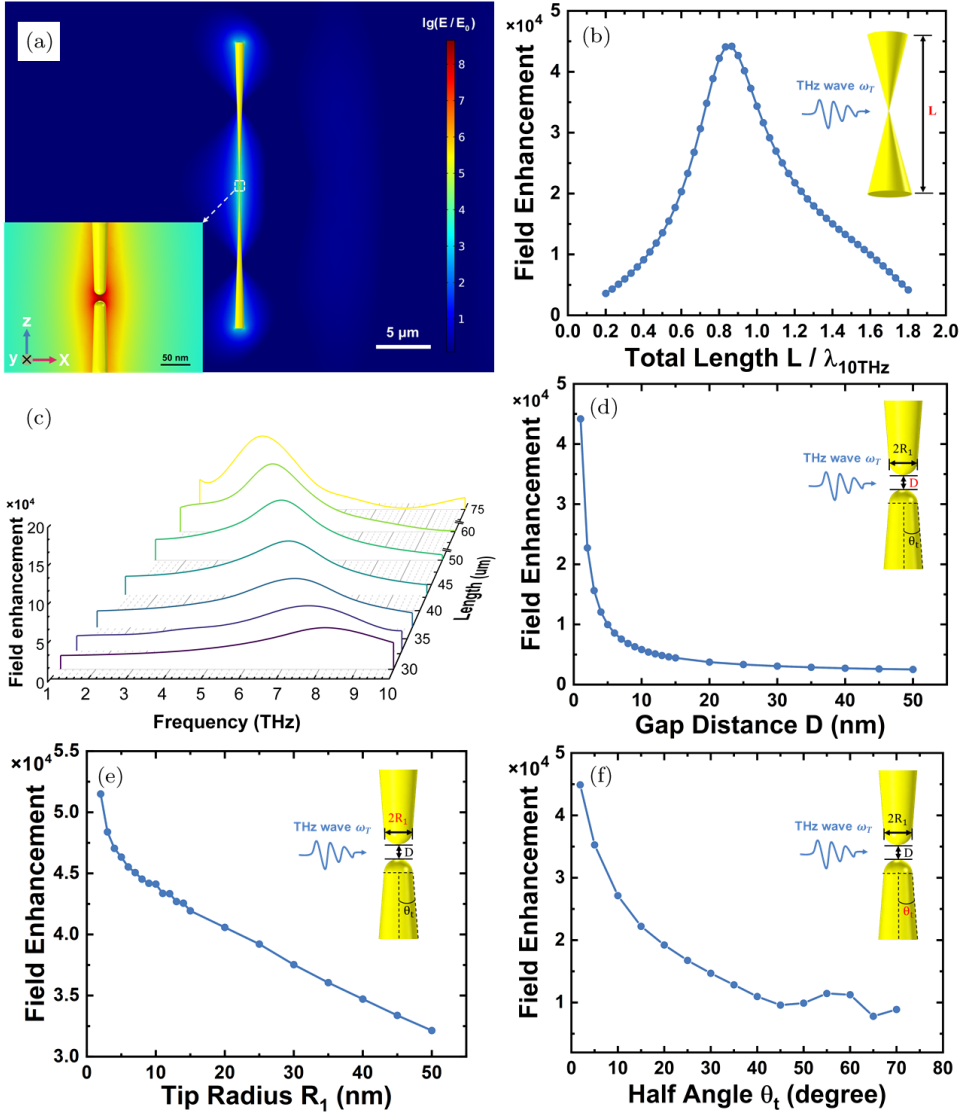
Fig. 3. (Color online) Numerical simulation of THz field enhancement. (a) The cross-section of the THz field distribution around the antenna in the plane containing the propagation and polarization axes. The inset zooms in the field distribution around the central part of the antenna. In this simulation, the geometrical parameters are $L = 26\,\mu m$, $D = 10\,nm$, $R_1 = 10\,nm$ and $\theta_t = 1.89°$. (b) shows the field enhancement E/E_0 versus the length L of the antenna. (c) shows the field enhancement is influenced by the relationship between the length of antenna and the frequency of the incident THz wave. (d)–(f) show the field enhancement versus geometrical parameters of antenna, including (d) the gap distance D, (e) the tip radius R_1, and (f) the half angle θ_t. Insets in (b) and (d)–(f) show the schematics of the simulated structure with changed parameter (marked with red color) and unchanged parameters (marked with black color). In these simulations, the initial geometrical parameters are $L = 26\,\mu m$, $D = 1\,nm$, $R_1 = 10\,nm$ and $\theta_t = 1.89°$.

Terahertz wave at 10 THz propagates along the x-axis with the polarization parallel to the antenna. The initial amplitude E_0 is set to $1\,\mathrm{V/m}$, and E/E_0 denotes the field enhancement. Different from optical domain, in THz domain, in order to satisfy antenna resonance, the total length L of the antenna should be the same order of magnitude as the THz wavelength, due to the certain relationship between the antenna length and resonant wavelength.[45–47] Therefore, the initial geometrical parameters are $L = 26\,\mu\mathrm{m}$, $D = 1\,\mathrm{nm}$, $R_1 = 10\,\mathrm{nm}$ and $\theta_t = 1.89°$. As shown in Fig. 3(a), the electric field distribution is surrounding the edge of the antenna, since the antenna is the perfect electric conductor for THz radiation and THz wave is hard to penetrate into it.[46] To show the details, the inset in Fig. 3(a) zooms in the field distribution around the central part of the antenna. It is obviously different from the distribution in Fig. 2(a) in optical domain, the electric field is not completely confined at the gap for the absence of LSPR mode, and THz wave can radiate with high energy due to antenna resonance as described in Ref. 48.

It is well known that the length of the antenna is crucial for the frequency-matched enhancement of resonant antenna.[49] The field enhancement affected by the various length of antenna is shown in Fig. 3(b). We set the frequency of the incoming THz wave to 10 THz ($\lambda = 30\,\mu\mathrm{m}$), and change the length L of the antenna. As shown in Fig. 3(b), the resonance wavelength leading to the peak of enhanced field is at $L = 26\,\mu\mathrm{m}$, and the highest field enhancement exceeds 44,000 times. Further, the relationship between the length of the antenna and the frequency of incoming THz wave is illustrated in Fig. 3(c), which has influence on the field enhancement. As shown in Fig. 3(c), each length of antenna is corresponding to a certain resonant frequency. For instance, the yellow curve denotes that the resonant antenna with a length of $75\,\mu\mathrm{m}$ is illuminated by THz wave with sweeping frequency, and the field enhancement achieves the maximum at resonant frequency around 3 THz. In addition, the resonance of antenna decreases and shows a redshift with the length of the antenna increasing.[43,46]

Figs. 3(d)–3(f) show that the field enhancement increases as the gap distance D, tip radius R_1 or half angle θ_t decreases respectively, which exhibits similar characteristics to optical field enhancement. As shown in Fig. 3(d), the field enhancement reaches more than 10,000 times when $D < 5\,\mathrm{nm}$, which is in good agreement with Ref. 48. In particular, Figs. 3(e) and 3(f) demonstrate that the field enhancement is influenced by the sharp tip of the antenna due to the lightning rod effect. Therefore, same as in optical domain, the field enhancement is highly influenced by the geometry of the gold antenna in THz domain, and it is feasible to optimize the antenna with appropriate geometrical parameters to enhance incident THz wave, thereby further improving the conversion efficiency of the SFG process.

3.3. Numerical simulation of SFG process

In this section, we perform the simulation of the nonlinear SFG process of optical wave and THz wave with FDTD method. Fig. 4(a) shows the schematic of SFG
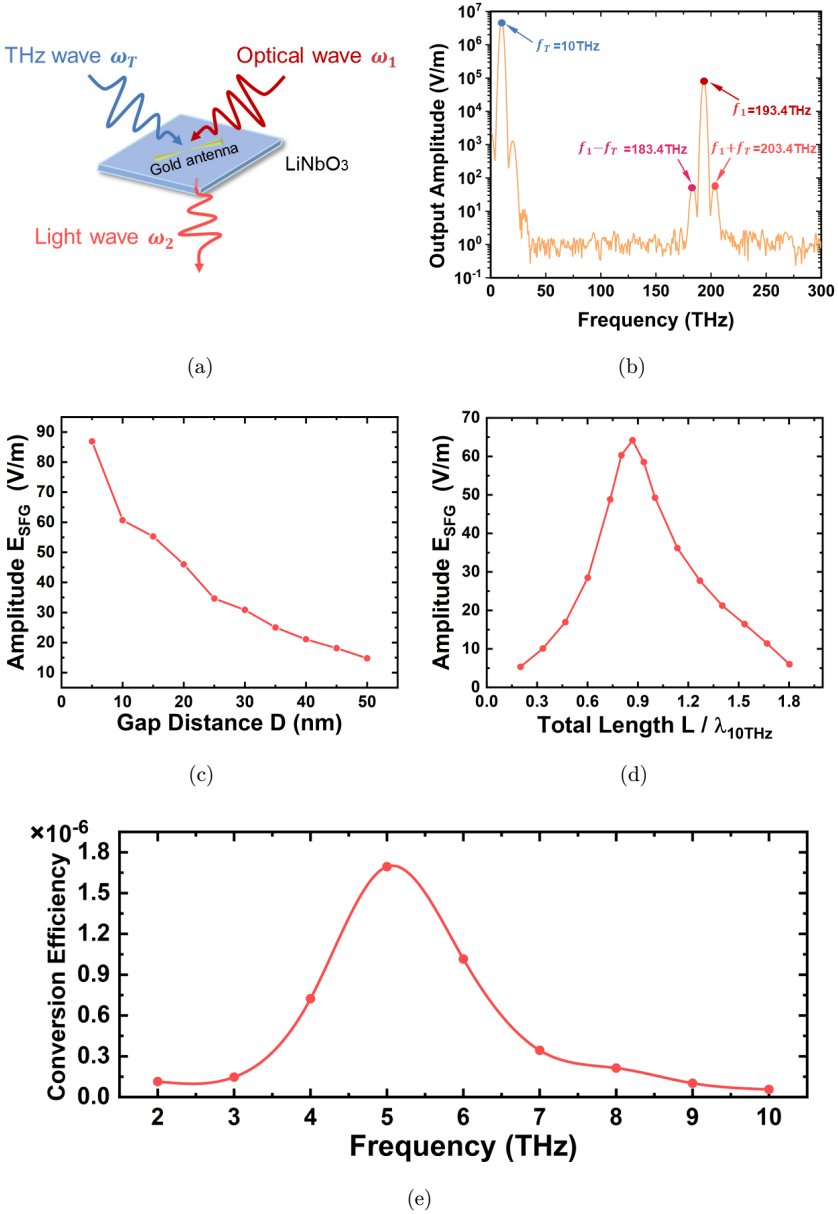
Fig. 4. The nonlinear SFG process simulated with the FDTD method. (a) Schematic illustration of the SFG process. (b) The spectrum of the output signal through SFG process, including optical wave at $f_1 = \omega_1/2\pi = 193.4$ THz ($\lambda = 1,550$ nm), THz wave at $f_T = \omega_T/2\pi = 10$ THz and the generated wave at $f_2 = \omega_2/2\pi = 203.4$ THz ($\lambda = 1,473$ nm). (c) The amplitude E_{SFG} of the generated wave ω_2 versus gap distance D. (d) The amplitude E_{SFG} of the generated wave ω_2 versus the total length L. In these simulations, the initial parameters are $L = 26\,\mu$m, $D = 10$ nm, $R_1 = 10$ nm and $\theta_t = 1.89°$. (e) The effective conversion efficiency $\eta = P_{\mathrm{SFG}}/P_{\mathrm{THz}}$ versus the frequency of incoming THz wave, where P_{SFG} is the output power of the generated wave, and P_{THz} is the initial power of THz wave incident on the antenna. In this simulation, the geometrical parameters are $L = 50\,\mu$m, $D = 10$ nm, $R_1 = 10$ nm and $\theta_t = 1.89°$.

process, in which the generated optical wave with a new frequency of ω_2 satisfies the energy conservation relationship $\omega_2 = \omega_1 + \omega_T$. The phase matching condition $\frac{n_2 \omega_2}{c} = \frac{n_1 \omega_1}{c} + \frac{n_T \omega_T}{c}$ can be satisfied automatically in simulation software, so there is no need to add additional simulation conditions. To demonstrate the SFG process, in this simulation, the power of optical wave at 1550 nm and THz wave at 10 THz are set to 1 mW and 10 μW, which are corresponding to the actual continuous-wave laser source and terahertz signal source, respectively, and the initial geometrical parameters of the gold antenna are set to $L = 26\,\mu$m, $D = 10$ nm, $R_1 = 10$ nm and $\theta_t = 1.89°$.

Fig. 4(b) presents the spectrum of the output signal through SFG process simulated by the FDTD method, where the incident THz wave is at 10 THz and the optical wave is at 193.4 THz ($\lambda = 1,550$ nm). The sidebands around the optical wave at 1,550 nm are generated by nonlinear DFG and SFG process, and the center frequency of the right band based on the SFG process is 203.4 THz ($\lambda = 1,473$ nm). In this simulation, the gap distance D is 10 nm, so the enhancement of incident waves is lower than that when $D = 1$ nm, but the amplitudes are still enhanced more than 10 times for optical field and 1,000 times for THz field, as shown in Fig. 4(b).

Figs. 4(c) and 4(d) show that the amplitude E_{SFG} of the generated optical wave ω_2 is influenced by the gap distance D and antenna length L. As shown in Fig. 4(c), the amplitude of the generated wave increases as the gap distance decreases. In Fig. 4(d), the amplitude reaches the maximum as the total length of the antenna approaches the wavelength of THz wave and yields a value of 64.2 V/m. In addition, the intensity of the generated wave is also affected by incident waves interacting in SFG process;[27] therefore, the trends in Figs. 4(c) and 4(d) are as same as those in optical domain and THz domain. Based on the discussion of previous sections, the lightning rod effect does influence the enhancement of electric fields, but the nano level changes of tip radius R_1 and half angle θ_t have less effect on the field enhancement than the changes of gap distance D and antenna length L, so the relationship between the amplitude of the generated wave and tip radius R_1 or half angle θ_t is not presented here.

To evaluate the efficiency of the up-conversion process, the efficiency for conversion of power from THz wave ω_T to the generated wave ω_2 can be defined by $\eta = P_{\text{SFG}}/P_{\text{THz}}$ (P_{SFG} is the output power of the generated wave; P_{THz} is initial power of THz wave incident on the antenna), so the expression has taken into account the enhancement of optical wave and THz wave and the efficiency of SFG process. In particular, the efficiency of the SFG process can be defined by[27]

$$\eta_{\text{SFG}} = \frac{P_{\text{SFG}}}{P_1^* \cdot P_{\text{THz}}^*} = \frac{P_{\text{SFG}}}{(\Gamma_1 \cdot P_1) \cdot (\Gamma_T \cdot P_{\text{THz}})}, \tag{1}$$

where $P_1^* = \Gamma_1 \cdot P_1$ is the enhanced optical wave ω_1 interacting in SFG process (Γ_1 is the enhancement factor in optical field; P_1 is the initial power of optical wave ω_1 incident on the antenna), and $P_{\text{THz}}^* = \Gamma_{\text{THz}} \cdot P_{\text{THz}}$ is the enhanced THz wave ω_T interacting in SFG process (Γ_T is the enhancement factor in THz field). Therefore,

the effective efficiency η can also be written as $\eta = \Gamma_1 \cdot \Gamma_T \cdot \eta_{\mathrm{SFG}} \cdot P_1$, which reveals that the effective efficiency increases as the power of the optical wave increases.[24,50]

Fig. 4(e) demonstrates that the effective efficiency η varies as the frequency of incident THz wave sweeps from 2 THz to 10 THz. In this simulation, the geometrical parameters are set to $L = 50\,\mu\mathrm{m}$, $D = 10\,\mathrm{nm}$, $R_1 = 10\,\mathrm{nm}$ and $\theta_t = 1.89°$. From Fig. 4(e), we observe that the efficiency η is more than 5×10^{-8}, and the maximum of the efficiency is obtained at 5 THz and more than 0.00016%, since the THz wave at 5 THz excites the antenna resonance and antenna effect in THz domain dominates the field enhancement.[48] Although the absorption and diffraction in the LiNbO$_3$ crystal affect the efficiency, the highest conversion efficiency we obtained is higher than those from other work using AgGaS$_2$ as nonlinear material when considering the same optical pump power.[21,24] In addition, as shown in Figs. 2(a) and 3(a), the THz spot size is large but the optical spot size is small, so the overlapping area between the optical field and the THz field may be small. The coupling efficiency of the two fields is calculated as 8.53%,[51] which may cause a waste of energy during the SFG process. To improve the efficiency of the SFG process, we consider optimizing our structure to expand the overlapping area. This can be done by integrating multiple nanostructures such as nanoantenna arrays and nanoparticles[29,47] around the center of the antenna, which can further improve the field enhancement and generate more optical hot spots due to the LSPR enhancement. Eventually, the overlap of the two fields can be expanded and the efficiency of the SFG process can be further improved.

In order to indirectly detect THz wave, we use a high-sensitive photodetector to receive the generated optical wave. Further, we evaluate the performance of the indirect detector with NEP, the effective NEP of the THz detection system NEP$_{\mathrm{eff}}$ is defined by[21]

$$\mathrm{NEP}_{\mathrm{eff}} = \mathrm{NEP}_{\mathrm{opt}} \cdot \frac{P_{\mathrm{THz}}}{P_{\mathrm{SFG}}} = \frac{\mathrm{NEP}_{\mathrm{opt}}}{\eta}, \qquad (2)$$

in which NEP$_{\mathrm{opt}}$ is the NEP of photodetector. We choose the commonly used FGA10 InGaAs APD with low NEP$_{\mathrm{opt}}$ of $2.5 \times 10^{-14}\,\mathrm{W}/\sqrt{\mathrm{Hz}}$ to detect the generated optical wave. Consequently, in the case of pump power of 1 W of incoming optical wave, the effective NEP of the detection system is calculated as $15.4\,\mathrm{pW}/\sqrt{\mathrm{Hz}}$ at 5 THz, which exceeds the NEP of uncooled commercial THz detectors, e.g., $1\,\mu\mathrm{W}/\sqrt{\mathrm{Hz}}$ of TP-Mili TERAPower, $1\,\mathrm{nW}/\sqrt{\mathrm{Hz}}$ of Terasense ultrafast Terahertz detector and $0.14\,\mathrm{nW}/\sqrt{\mathrm{Hz}}$ of GC-1T Golay Cell.

In this study, the NEP of the detector is limited by the efficiency of the up-conversion process, and the NEP of InGaAs APD operating at communication window of $1.5\,\mu\mathrm{m}$ is higher than that of Si APD operating at window of 800 nm (e.g., $0.86\,\mathrm{fW}/\sqrt{\mathrm{Hz}}$ of Perkin-Elmer C30902S Si APD). Therefore, the better performance of the detector is available through selecting optical wave at 800 nm to interact in the SFG process and improving input power without saturation, or choosing better

nonlinear material to reduce the absorption for THz wave.[26] In addition, as shown in Fig. 4(e), the effective bandwidth may not cover a broad spectrum from THz pulse,[52,53] so the scheme needs to be optimized for broadband THz field detection. We consider replacing the single antenna in previous scheme with multi-antenna structure consisting of several antennas with different lengths. Fig. 3(c) reveals that the antenna resonance varies as the length of the antenna changes, and Fig. 4(e) demonstrates that the resonance of the structure mainly depends on the antenna effect in THz domain. Therefore, when the THz pulses are incident on the multi-antenna structure, the interaction will induce multiple resonances upon the spectrum of incident THz pulses. Accordingly, the effective bandwidth of the optimized detector can be expanded and support broadband THz field detection.

4. Conclusion

We have proposed a THz detection scheme based on nonlinear SFG process enhanced by the gold antenna. The results of numerical simulations with the FEA method demonstrate that the field enhancement of optical wave and THz wave is influenced by the geometry of the antenna, which supports LSPR enhancement for optical field and antenna resonance for THz field. In particular, due to the sharp tip, the lightning rod effect can also strengthen the electric field. In addition, the results of simulation on SFG process with FDTD method show that the conversion efficiency of the up-conversion process exceeds those of many other technologies. By comparison, the NEP of $15.4\,\mathrm{pW}/\sqrt{\mathrm{Hz}}$ of our detector is much lower than many commercial THz detectors. Therefore, it indicates that the THz detector based on the up-conversion process can operate at room temperature with good performance benefiting from sensitive optical detectors.[23]

In order to achieve the lower NEP of the detector, it is favorable to design the antenna with optimum geometrical parameters and improve the pump power without saturation. In addition, our proposed single-antenna structure can be further optimized to be multi-antenna structure for broadband THz field detection. The scheme can be exploited to improve the efficiency of other parametric conversion processes in wide bandwidth. Furthermore, besides the applications in THz detection, due to the combination between THz domain and optical domain, we also expect our scheme can be beneficial for the realization of THz wireless link integrated into optical link for future wireless communication.

References

1. P. T. Dat, A. Kanno, T. Umezawa, N. Yamamoto and T. Kawanishi, Millimeter- and terahertz-wave radio-over-fiber for 5G and beyond, *2017 IEEE Photonics Society Summer Topical Meeting Series*, San Juan, PR, United States (July 2017), pp. 165–166.

2. S. Li, L. D. Xu and S. Zhao, 5G internet of things: A survey, *J. Ind. Inf. Integr.* **10** (2018) 1.

3. R. Zhou, C. Wang, W. Xu and L. Xie, Biological applications of terahertz technology based on nanomaterials and nanostructures, *Nanoscale* **11** (2019) 3445.

4. J. Qin, Y. Ying and L. Xie, The detection of agricultural products and food using terahertz spectroscopy: A review, *Appl. Spectrosc. Rev.* **48** (2013) 439.

5. M. Tonouchi, Cutting-edge terahertz technology, *Nat. Photonics* **1** (2007) 97.

6. P. Yang, Y. Xiao, M. Xiao and S. Li, 6G wireless communications: Vision and potential techniques, *IEEE Netw.* **33** (2019) 70.

7. M. Giordani, M. Polese, M. Mezzavilla, S. Rangan and M. Zorzi, Toward 6G networks: Use cases and technologies, *IEEE Commun. Mag.* **58** (2020) 55.

8. J. Federici and L. Moeller, Review of terahertz and subterahertz wireless communications, *J. Appl. Phys.* **107** (2010) 111101.

9. I. F. Akyildiz, J. M. Jornet and C. Han, Terahertz band: Next frontier for wireless communications, *Phys. Commun.* **12** (2014) 16.

10. T. Kürner and S. Priebe, Towards THz communications - Status in research, standardization and regulation, *J. Infrared Millim. Terahertz Waves* **35** (2014) 53.

11. A. V. Raisanen, Challenges of terahertz, *The Second European Conf. Antennas and Propagation 2007*, Edinburgh, United Kingdom, November 2007, pp. 1–4.

12. B. Ferguson and X.-C. Zhang, Materials for terahertz science and technology, *Nat. Mater.* **1** (2002) 26.

13. M. Hangyo, Development and future prospects of terahertz technology, *J. Appl. Phys.* **54** (2015) 120101.

14. J.-S. Rieh, THz detectors and related topics, in *Introduction to Terahertz Electronics*, Chapter 2, ed. J.-S. Rieh (Springer, Cham, 2021) pp. 95–161.

15. M. Zerbini, A. Doria, G. P. Gallerano, E. Giovenale and G. Galatola-Teka, Far infrared and THz detectors: Principles of operation and figures of merit, *2018 43rd Int. Conf. Infrared, Millimeter, and Terahertz Waves*, Nagoya, Japan, September 2018, pp. 1–2.

16. J. Y. Suen, K. Fan, J. Montoya, C. Bingham, V. Stenger, S. Sriram and W. J. Padilla, Multifunctional metamaterial pyroelectric infrared detectors, *Optica* **4** (2017) 276.

17. Y. Zhang, X. Zhang, S. Li, J. Gu, Y. Li, Z. Tian, C. Ouyang, M. He, J. Han and W. Zhang, A broadband THz-TDS system based on DSTMS emitter and LTG InGaAs/InAlAs photoconductive antenna detector, *Sci. Rep.* **6** (2016) 26949.

18. X. G. Guo, J. C. Cao, R. Zhang, Z. Y. Tan and H. C. Liu, Recent progress in terahertz quantum-well photodetectors, *IEEE J. Sel. Top. Quantum Electron.* **19** (2013) 8500508.

19. S. Komiyama, Single-photon detectors in the terahertz range, *IEEE J. Sel. Top. Quantum Electron.* **17** (2011) 54.

20. H. Schneider, H. C. Liu, S. Winnerl, C. Y. Song, M. Walther and M. Helm, Terahertz two-photon quantum well infrared photodetector, *Opt. Express* **17** (2009) 12279.

21. K. Karstad, A. Stefanov, M. Wegmuller, H. Zbinden, N. Gisin, T. Aellen, M. Beck and J. Faist, Detection of mid-IR radiation by sum frequency generation for free space optical communication, *Opt. Switz.* **43** (2005) 537.

22. G. Santamaria-Botello, A. Rivera-Lavado, S. Preu, F. Sedlmeir, D. Lioubtchenko, H. Schwefel, D. Segovia-Vargas and L. E. G. Munoz, Sub-THz photon counting receiver working at room temperature for polarization measurements of the cosmic microwave

background radiation, *2016 10th Eur. Conf. Antennas and Propagation*, Davos, Switzerland (2016), pp. 1–5.

23. Y. Takida, K. Nawata, S. Suzuki, M. Asada and H. Minamide, Nonlinear optical detection of terahertz-wave radiation from resonant tunneling diodes, *Opt. Express* **25** (2017) 5389.

24. Y.-P. Tseng, C. Pedersen and P. Tidemand-Lichtenberg, Upconversion detection of long-wave infrared radiation from a quantum cascade laser, *Opt. Mater. Express* **8** (2018) 1313.

25. S. Ummethala, T. Harter, K. Koehnle, Z. Li, S. Muehlbrandt, Y. Kutuvantavida, J. Kemal, P. Marin-Palomo, J. Schaefer, A. Tessmann, S. K. Garlapati, A. Bacher, L. Hahn, M. Walther, T. Zwick, S. Randel, W. Freude and C. Koos, THz-to-optical conversion in wireless communications using an ultra-broadband plasmonic modulator, *Nat. Photonics* **13** (2019) 519.

26. S. Hayashi, K. Nawata, T. Taira, J. Shikata, K. Kawase and H. Minamide, Ultrabright continuously tunable terahertz-wave generation at room temperature, *Sci. Rep.* **4** (2014) 5045.

27. R. W. Boyd, *Nonlinear Optics*, 4th edn. (Academic Press, United States, 2020).

28. Y. X. Ge, J. J. Cao, Z. H. Shen, Y. L. Zheng, X. F. Chen and W. J. Wan, Terahertz wave generation by plasmonic-enhanced difference-frequency generation, *J. Opt. Soc. Am. B* **31** (2014) 1533.

29. H. Aouani, M. Rahmani, M. Navarro-Cía and S. A. Maier, Third-harmonic-upconversion enhancement from a single semiconductor nanoparticle coupled to a plasmonic antenna, *Nat. Nanotechnol.* **9** (2014) 290.

30. V. Khoshdel and M. Shokooh-Saremi, Plasmonic nano bow-tie arrays with enhanced LSPR refractive index sensing, *Micro Nano Lett.* **14** (2019) 566.

31. P. Mühlschlegel, H.-J. Eisler, O. J. F. Martin, B. Hecht and D. W. Pohl, Resonant optical antennas, *Science* **308** (2005) 1607.

32. A. Kinkhabwala, Z. Yu, S. Fan, Y. Avlasevich, K. Müllen and W. E. Moerner, Large single-molecule fluorescence enhancements produced by a bowtie nanoantenna, *Nat. Photonics* **3** (2009) 654.

33. S.-G. Park, K. H. Jin, M. Yi, J. C. Ye, J. Ahn and K.-H. Jeong, Enhancement of terahertz pulse emission by optical nanoantenna, *ACS Nano* **6** (2012) 2026.

34. P. R. West, S. Ishii, G. V. Naik, N. K. Emani, V. M. Shalaev and A. Boltasseva, Searching for better plasmonic materials, *Laser Photonics Rev.* **4** (2010) 795.

35. P. Verma, Tip-enhanced Raman spectroscopy: Technique and recent advances, *Chem. Rev.* **117** (2017) 6447.

36. J. B. Pendry, L. Martín-Moreno and F. J. Garcia-Vidal, Mimicking surface plasmons with structured surfaces, *Science* **305** (2004) 847.

37. R. B. Kohlhaas, A. Rehn, S. Nellen, M. Koch, M. Schell, R. J. B. Dietz and J. C. Balzer, Terahertz quasi time-domain spectroscopy based on telecom technology for 1550 nm, *Opt. Express* **25** (2017) 12851.

38. P. B. Johnson and R. W. Christy, Optical constants of the noble metals, *Phys. Rev. B* **6** (1972) 4370.

39. K. B. Crozier, A. Sundaramurthy, G. S. Kino and C. F. Quate, Optical antennas: Resonators for local field enhancement, *J. Appl. Phys.* **94** (2003) 4632.

40. K. L. Kelly, E. Coronado, L. L. Zhao and G. C. Schatz, The optical properties of metal nanoparticles: The influence of size, shape, and dielectric environment, *J. Phys. Chem. B* **107** (2003) 668.

41. P. F. Liao and A. Wokaun, Lightning rod effect in surface enhanced Raman scattering, *J. Chem. Phys.* **76** (1982) 751.

42. N. Anderson, A. Bouhelier and L. Novotny, Near-field photonics: Tip-enhanced micros-copy and spectroscopy on the nanoscale, *J. Opt. Pure Appl. Opt.* **8** (2006) S227.
43. Y. M. Wu, L. W. Li and B. Liu, Geometric effects in designing bow-tie nanoantenna for optical resonance investigation, *2010 Asia-Pacific Int. Symp. Electromagnetic Compat-ibility*, Beijing, China, April 2010, pp. 1108–1111.
44. M. A. Ordal, R. J. Bell, R. W. Alexander, L. L. Long and M. R. Querry, Optical properties of Au, Ni, and Pb at submillimeter wavelengths, *Appl. Opt.* **26** (1987) 744.
45. P. Roelli, D. Martin-Cano, T. J. Kippenberg and C. Galland, Molecular platform for frequency upconversion at the single-photon level, *Phys. Rev. X* **10** (2020) 031057.
46. C. Zhang, Z. Ninkov, G. Fertig, R. Kremens, A. Sacco, D. Newman, K. Fourspring, P. Lee, Z. Ignjatovic, J. Pipher, C. McMurtry and J. Dayalu, Optical simulation of terahertz antenna using finite difference time domain method, *Terahertz Physics, Devices, and Systems IX: Advanced Applications in Industry and Defense*, Baltimore, United States, (International Society for Optics and Photonics, May 2015), pp. 94830D.
47. A. Toma, S. Tuccio, M. Prato, F. De Donato, A. Perucchi, P. Di Pietro, S. Marras, C. Liberale, R. Proietti Zaccaria, F. De Angelis, L. Manna, S. Lupi, E. Di Fabrizio and L. Razzari, Squeezing terahertz light into nanovolumes: Nanoantenna enhanced terahertz spectroscopy (NETS) of semiconductor quantum dots, *Nano Lett.* **15** (2015) 386.
48. A. Haidary, Y. Miyahara and P. Grütter, Antenna and plasmonic properties of scanning probe tips at optical and terahertz regimes, in *Proc. 2014 COMSOL Conference*, Boston, United States, September 2014.
49. W. L. Stutzman and G. A. Thiele, *Antenna Theory and Design*, 3rd edn. (John Wiley & Sons, United States, 2012).
50. G. Grinblat, Y. Li, M. P. Nielsen, R. F. Oulton and S. A. Maier, Efficient third harmonic generation and nonlinear subwavelength imaging at a higher-order anapole mode in a single germanium nanodisk, *ACS Nano* **11** (2017) 953.
51. M. Fadhali, Saktioto, J. Zainal, Y. Munajat, J. Ali and R. A. Rahman, Mode matching for efficient laser diode to single mode fiber coupling, *Int. Workshop and Conf. Photonics and Nanotechnology 2007*, Pattaya, Thailand, April 2008, pp. 67930G.
52. T. Seifert, S. Jaiswal, U. Martens, J. Hannegan, L. Braun, P. Maldonado, F. Freimuth, A. Kronenberg, J. Henrizi, I. Radu, E. Beaurepaire, Y. Mokrousov, P. M. Oppeneer, M. Jourdan, G. Jakob, D. Turchinovich, L. M. Hayden, M. Wolf, M. Münzenberg, M. Kläui and T. Kampfrath, Efficient metallic spintronic emitters of ultrabroadband terahertz radiation, *Nat. Photonics* **10** (2016) 483.
53. C. Zhou, Y. P. Liu, Z. Wang, S. J. Ma, M. W. Jia, R. Q. Wu, L. Zhou, W. Zhang, M. K. Liu, Y. Z. Wu and J. Qi, Broadband terahertz generation via the interface inverse Rashba-Edelstein effect, *Phys. Rev. Lett.* **121** (2018) 086801.